MNRAS **000**, 1–10 (2015) Preprint 4 December 2015 Compiled using MNRAS LATEX style file v3.0

NuSTAR discovery of a cyclotron absorption line in the transient X-ray pulsar 2S 1553−542

Sergey S. Tsygankov,[1⋆] Alexander A. Lutovinov,[2] Roman A. Krivonos,[2] Sergey V. Molkov,[2] Peter J. Jenke,[3] Mark H. Finger,[4] and Juri Poutanen[1,5]

[1] *Tuorla Observatory, Department of Physics and Astronomy, University of Turku, Väisäläntie 20, FI-21500 Piikkiö, Finland*
[2] *Space Research Institute of the Russian Academy of Sciences, Profsoyuznaya Str. 84/32, Moscow 117997, Russia*
[3] *University of Alabama in Huntsville, 301 Sparkman Drive, Huntsville, AL 35899, USA*
[4] *Universities Space Research Association, National Space Science and Technology Center, 320 Sparkman Drive, Huntsville, AL 35805, USA*
[5] *Nordita, KTH Royal Institute of Technology and Stockholm University, Roslagstullsbacken 23, SE-10691 Stockholm, Sweden*

arXiv:1512.00851v1 [astro-ph.HE] 2 Dec 2015

Accepted 2015 December 2. Received 2015 November 26; in original form 2015 September 19.

ABSTRACT

We report results of a spectral and timing analysis of the poorly studied transient X-ray pulsar 2S 1553−542 using data collected with the *NuSTAR* and *Chandra* observatories and the *Fermi*/GBM instrument during an outburst in 2015. Properties of the source at high energies (> 30 keV) are studied for the first time and the sky position had been essentially improved. The source broadband spectrum has a quite complicated shape and can be reasonably described by a composite model with two continuum components – a black body emission with the temperature about 1 keV at low energies and a power law with an exponential cutoff at high energies. Additionally an absorption feature at ~ 23.5 keV is discovered both in phase-averaged and phase-resolved spectra and interpreted as the cyclotron resonance scattering feature corresponding to the magnetic field strength of the neutron star $B \sim 3 \times 10^{12}$ G. Based on the *Fermi*/GBM data the orbital parameters of the system were substantially improved, that allowed us to determine the spin period of the neutron star $P = 9.27880(3)$ s and a local spin-up $\dot{P} \simeq -7.5 \times 10^{-10}$ s s^{-1} due to the mass accretion during the *NuSTAR* observations. Assuming accretion from the disk and using standard torque models we have estimated the distance to the system $d = 20 \pm 4$ kpc.

Key words: accretion, accretion discs – magnetic fields – stars: individual: 2S 1553−542 – X-rays: binaries.

1 INTRODUCTION

The transient source 2S 1553−542 belongs to the numerous subclass of the accreting X-ray pulsars with Be optical companions (BeXRP). It was discovered by *SAS-3* observatory during the Galactic plane survey in 1975 (Walter 1976). Later on the transient nature of the source was established as well as strong pulsations with the period of 9.3 s and amplitude of $\sim 80\%$ were found (Kelley, Ayasli, & Rappaport 1982). Using the same data an orbital period of the binary system was measured $P_{\rm orb} = 30.6 \pm 2.2$ d and a suggestion that 2S 1553−542 is likely a Be/X-ray binary system has been made (Kelley, Rappaport, & Ayasli 1983). It is important to note that no optical counterpart was directly determined for 2S 1553−542 so far (however see below).

Second time after the discovery 2S 1553−542 came into the view of X-ray instruments during the outburst in 2007–2008 (Krimm et al. 2007). An intensive monitoring of this outburst with the *RXTE* observatory allowed to improve orbital parameters of the system and to trace the spectral evolution in the energy range 2.5–30 keV (Pahari & Pal 2012). Particularly it was shown that the source spectra in all available intensity states can be well fitted with the combination of a black-body component (with temperature varying between 2.5 and 4 keV) and a broken power-law component. The iron emission line at ~ 6.5 keV and a strong photoelectric absorption corresponding to hydrogen column density of $N_{\rm H} \sim 5 \times 10^{22}$ cm^{-2} were also required by the fit.

The third episode when 2S 1553−542 has undergone an outburst was observed in the beginning of 2015. The increase of the flux seen in the *MAXI*/GSC data was reported by Sugizaki et al. (2015). An estimated starting date of the activity was around 2015 January 28 (MJD 57050).

In this paper we describe results of the comprehensive spectral and temporal analysis of the high quality data

⋆ E-mail: stsygankov@gmail.com

© 2015 The Authors

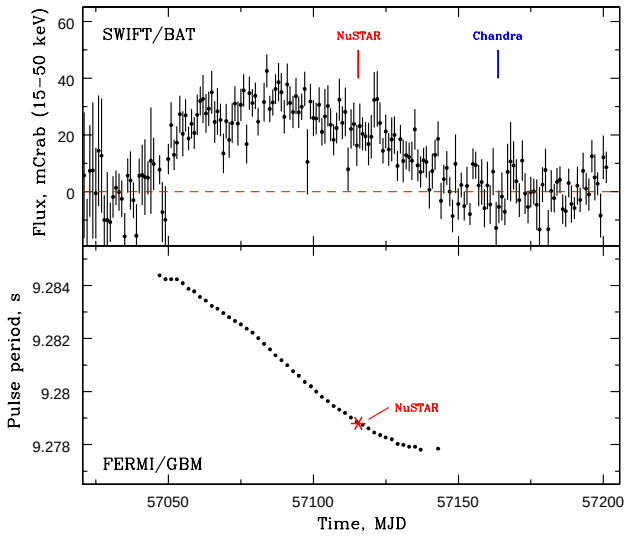

Figure 1. *Top*: *Swift*/BAT light curve of 2S 1553−542 in the 15–50 keV energy band (black points). Flux is given in units of mCrab (1 mCrab = 1.4×10^{-11} erg s^{-1} cm^{-2}). Times of the *NuSTAR* and *Chandra* observations are marked. *Bottom:* Evolution of the pulsar spin period over the outburst as seen by the *Fermi* Gamma-Ray Burst Monitor (GBM). Asterisk shows corrected for the orbital motion period measured by *NuSTAR* (see text for the details).

collected by the *NuSTAR* observatory during the declining phase of this outburst (MJD 57115.48). Main goal was to explore the source properties at high energies (above 30 keV) for the first time.

2 OBSERVATIONS AND DATA REDUCTION

2.1 *NuSTAR* observations

The *Nuclear Spectroscopic Telescope Array (NuSTAR)* (Harrison et al. 2013), launched on 13 June 2012, is the first orbital X-ray focusing telescope operating at energies above 10 keV. The observatory consists of two co-aligned identical X-ray telescope systems operating in a wide energy range from 3 to 79 keV with angular resolution of 18″(FWHM) and half-power diameter (HPD) of 58″. Spectral energy resolution of 400 eV (FWHM) at 10 keV is provided by independent solid state CdZnTe pixel detector units for each telescope, usually referred as focal plane module A and B (FPMA and FPMB).

NuSTAR performed a TOO observation of 2S 1553−542 in the declining phase of the outburst (MJD 57115.4834, see Fig. 1) with a total exposure time of 27 ks (Obs. ID 90101002002). The source was relatively bright demonstrating net count rate of about 20 cts s^{-1} on both FPMA and FPMB. We did not notice any special issues related to the high count rate of the source in the following analysis. The source covered large area of the FOV (Fig. 2) because the *NuSTAR* PSF has wide wings (Harrison et al. 2013; An et al. 2014). The data were reduced using the NuSTARDAS pipeline version v1.4.1 (28 May 2014) and CALDB version 20150612.

In order to perform a barycentric corrections it is necessary to know the source position with a good accuracy. Observations with the *Chandra* observatory, performed on 2015 May 21 (MJD 57163.68; ObsID. 17662), allowed us to measure it as R.A.= $15^{\rm h}57^{\rm m}48\overset{\rm s}{.}3$, Dec.= $-54^\circ24'53\overset{''}{.}1$ (J2000) with an 1″ uncertainty (90%). Note, that these *Chandra* observations as well as observations with the *Swift*/XRT telescope were used to determine the optical counterpart in the system and to measure the absorption value (Lutovinov et al. 2015b). The latter is important for the analysis of the *NuSTAR* data as it works above 3 keV and not very sensitive to the small or moderate absorption values. We would like to remind here that a quite high photoabsorption ($4-5\times10^{22}$ cm^{-2}) was required by Pahari & Pal (2012) to describe the source spectra, obtained with the *RXTE* observatory (it operates also above 3 keV). Such high values are quite atypical for BeXRPs, whose spectra do not demonstrate usually a strong absorption. Our analysis of *Chandra* and *Swift*/XRT data in soft X-ray band shows lower photoabsorption value in the source spectrum around $\simeq 2.3\times10^{22}$ cm^{-2} (Lutovinov et al. 2015b), which was fixed in the following spectral analysis of the *NuSTAR* data. Note, that it is only slightly higher, than the estimations of the galactic interstellar absorption in this direction $\sim 1.6-1.9\times10^{22}$ cm^{-2} (Dickey & Lockman 1990; Kalberla et al. 2005).

We extracted spectra using NUPRODUCTS script provided by the NuSTARDAS pipeline. The source spectrum was extracted within 120″ aperture around the source position as shown in Fig. 2, which constitutes 92% of PSF enclosed energy (see, e.g., An et al. 2014). The *NuSTAR* background varies across the FOV due to the different stray light (also called "aperture") background components: individual bright X-ray sources, isotropic extragalactic Cosmic X-ray Background (CXB) and Galactic X-ray Ridge Emission (GRXE; Wik et al. 2014). The field around 2S 1553−542 does not contain stray light from nearby Galactic sources, but it has CXB and GRXE components in the background, because 2S 1553−542 is located in the Galactic plane (l^{II}=−32.056, b^{II}=−0.857). We used suite of IDL routines NUSKYBGD (Wik et al. 2014) to model all the known background components (instrumental, CXB and GRXE) in the source-free region outside the green dashed circle (R=330″) shown in Fig. 2. This model was utilized to estimate background spectrum at the position of the source.

2.2 *Fermi*/GBM and *Swift*/BAT observations

Fermi Gamma Ray Burst Monitor (GBM) is an all sky monitor whose primary objective is to extend the energy range over which gamma-ray bursts are observed in the Large Area Telescope (LAT) on *Fermi* (Meegan et al. 2009). GBM consists of 12 NaI detectors with a diameter of 12.7 cm and a thickness of 1.27 cm and two BGO detectors with a diameter and thickness of 12.7 cm. The NaI detectors have an energy range from 8 keV to 1 MeV while the BGO's extend the energy range to 40 MeV.

The *Swift* Burst Alert Telescope (BAT) is a hard X-ray monitor that has a field-of-view of 1.4 steradians and its array of CdZnTe detectors are sensitive in 15–150 keV range Krimm et al. (2013). It is a coded aperture instrument with a detector area of 5200 cm^2. We use the BAT transient

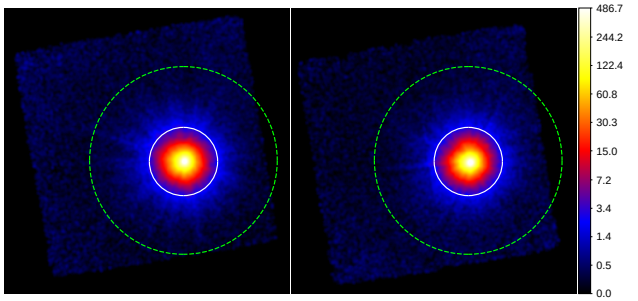

Figure 2. Exposure-corrected sky images of 2S 1553−542 from FPMA (left) and FPMB (right) in 3 − 79 keV energy band. The images have been smoothed by a Gaussian kernel with 9′′ width and color-coded in logarithmic scale for convenience. The color bar on the right indicates the units of the images expressed in 10^{-4} cts pix^{-1} s^{-1}. The solid white circle (120′′ radius) denotes region for the source extraction. The NUSKYBGD background model has been calibrated in the area outside the green dashed circle (330′′ radius).

monitor results[1] (15–50 keV), provided by the BAT team in order to model the torque imparted to the neutron star by the accreted material.

GBM Channel 1 (12–25 keV) CTIME data from 57020–57145 MJD is binned to 250 ms and fit to a semi-empirical background model. The background model is subtracted and pulsed flux and frequencies for 2S 1553-542 are extracted from the data by modeling its Fourier components (Jenke et al. 2012; Finger et al. 1999).

3 RESULTS

As can be seen from Fig. 1(a) total duration of the analysed outburst is around 3.5 months covering more than 3 complete binary orbital cycles. Such a duration is typical for Type II outbursts from BeXRPs. These events are caused by the non-stationary increase of the amount of matter in the Be circumstellar disc. Peak luminosities can be much higher than 10^{37} erg s^{-1} (for a review, see Reig 2011).

3.1 Orbital parameters

We have determined an orbital model for 2S 1553−542 using the *Fermi*/GBM and the *Swift*/BAT data. Typically, after correcting the pulse arrival times for Earth's motion, one can use the doppler boosted frequencies of the pulses to fit a model for the binary system. Material accreted onto a neutron star surface or collected in an accretion disk threaded by the neutron star's magnetic field transfers angular momentum to the neutron star. Disentangling this intrinsic spin-up from the orbital signature is challenging. A solution to this problem is to model the intrinsic spin-up using a proxy for the system's X-ray luminosity. The luminosity is a function of mass accretion which is related to the torque imposed on the neutron star. Rappaport & Joss (1977) showed that, at high luminosity, the intrinsic spin-up, $\dot{\nu}$, is proportional to $L^{6/7}$ when accretion is mediated through a disk. The proportionality constant is a function of mass, radius, moment of inertia, distance and magnetic field of the neutron star along with a few parameters describing accretion and emission efficiency. When connecting multiple outburst with the same torque model, it is necessary to include a spin-down term to account for angular momentum losses during quiescence.

Table 1. Orbital Ephemeris for 2S 1553−542.

Orbital Period	31.303(27)	days
$T_{\pi/2}$	2457089.421(19)	days
$a_x \sin i$	201.25(84)	lt-sec
Eccentricity	0.0351(22)	
Longitude of periastron	163.4(35)	degrees
χ^2	66.3 / 38 d.o.f.	

A search for frequency and frequency rate is performed using pulse profiles from GBM folded over a two day interval. Each frequency epoch is chosen as the mean exposure-weighted observation time. The epochs are barycentered using the JPL Planetary ephemeris DE200 (Standish 1990). BAT survey data (15–50 keV) for 2S 1553−542 are used as a proxy for the source luminosity and to model the intrinsic spin-up rate. In order to eliminate under-constrained and over-constrained rates, only BAT rates with errors greater than 10^{-3} and less than 0.05 are used. This spin-up model along with the line of sight delay associated with the binary orbit from Deeter, Boynton, & Pravdo (1981) is used to model the barycentered arrival times. Minimization of the χ^2 fit of the barycentric frequencies and the BAT rates is performed using the Levenberg-Marquart method and is of the form:

$$\chi^2 = \sum_i (f_i - (\dot{\nu_i}(1-\beta_i))^2 \quad ; i = 0, n-1 \qquad (1)$$
$$+ \sum_i (X_i - \dot{\nu_i}/m)^2 \quad ; i = 0, n-2 \qquad (2)$$

where β_i is the orbital redshift factor at time t_i which is a function of the orbital elements, f_i is the measured barycentric frequency at time t_i which is the frequency epoch of the search interval i. Each epoch is chosen as the mean exposure-weighted observation time. X_i is the average value of $R^{6/7}$ between t_i and t_{i+1} and R is the BAT rate. The model parameter ν_i is the orbitally corrected frequency at time t_i and $\dot{\nu_i}$ is $(\nu_{i+1} - \nu_i)/(t_{i+1} - t_i)$.

The updated orbital model is used in a new search for frequencies and frequency rates recursively until the orbital solution becomes stationary. The final fit resulted in a $\chi^2 = 66.3$ with 38 d.o.f. Variability in the pulse profile within the two day integration interval contributed to errors in the measured frequency. In addition, changes in the emission beam within the integration interval or systematically throughout the outburst is expected to produce systematic errors in the BAT rates used to model the spin-up. In order to adjust the errors on the orbital parameters to account for these issues, the errors are increased by 1.35 which results in a orbital fit with a reduced $\chi^2 \sim 1$.

This ephemeris is orbitally phase connected, within 2.7 ± 2.3 days, to the orbit determined in Pahari & Pal (2012) from the 2008 outburst. Spin down between the 2008 outburst and 2015 outburst is ∼ 6.5 cycles per day.

The frequency history, pulsed flux and ephemeris for

[1] http://heasarc.gsfc.nasa.gov/docs/swift/results/transients/

this source and all other sources monitored by the GBM Pulsar Monitoring team may be found at the GBM pulsar website[2].

3.2 Pulse period and profile

To determine the mean pulse period and its uncertainty using the *NuSTAR* observation we took the barycentered light curve in the wide energy band (3–79 keV) and based on that generated a set of 10^4 trial light curves. For each light curve we found a pulse period and got a distribution of these trial periods. Individual pulse periods in each light curve were obtained using EFSEARCH procedure from FTOOLS package. The mean value of this distribution was taken as proper pulse period of 2S 1553−542 and the standard deviation – as the corresponding 1σ uncertainty (see, e.g., Boldin, Tsygankov, & Lutovinov 2013).

Following this procedure we obtained the spin period $P_{\rm spin} = 9.282204(2)$ s in the raw data. This corresponds to the intrinsic spin period value $P_{\rm spin} = 9.27880(3)$ s after the correction for the orbital motion using orbital parameters listed in Section 3.1. An uncertainty for the intrinsic period value was calculated using Monte-Carlo simulations taking into account uncertainties in the orbital parameters and using standard relations between the pulse period and ephemeris. Spin period from the *NuSTAR* data is shown in the lower panel of Fig. 1 by the asterisk. Interestingly, it is roughly equal to the period value at the moment of the source discovery around 40 years ago. In spite of significant spin-up observed during the outburst episode (see bottom panel of Fig.1) the period constancy over decades is not surprising due to rarity of such accretion events and slow spin-down between them. Very similar picture is seen in many other rarely bursting transient BeXRPs, like 4U 0115+63, V 0332+53, A 0535+262 and others.[2]

Pulse profile shape carries useful information about geometrical properties of the emitting area at the neutron star surface, whereas its dependence on energy reflects physical properties of matter–radiation interaction. Following Krivonos et al. (2015) instead of analysing light curves from modules FPMA and FPMB independently we combined them in order to get better statistics.

Pulse profile has a single-peak shape with a barely noticeable dependence on energy. Figure 3 illustrates evolution of the normalized for the mean flux pulse profile over five energy bands: 3–7, 7–18, 18–30, 30–50, and 50–79 keV (from top to bottom). Three main features can be distinguished: main maximum, main minimum and energy-dependent wing, appearing in 18–30 keV energy band. In the figure these features are shown by short-dashed line, long-dashed line and dotted line, correspondingly.

Most obviously pulse profile dependence on energy is illustrated by hardness ratios shown in Fig. 4. Quite complicated structure of all four ratios is mainly defined by energy dependence of the main peak. Namely, an additional component is appearing in 18–30 keV energy band at phases ∼0.1–0.2 (shown by dotted line). Interestingly, this component disappears at higher energies. This is clearly seen from the decrease of the hardness ration below the level of unity

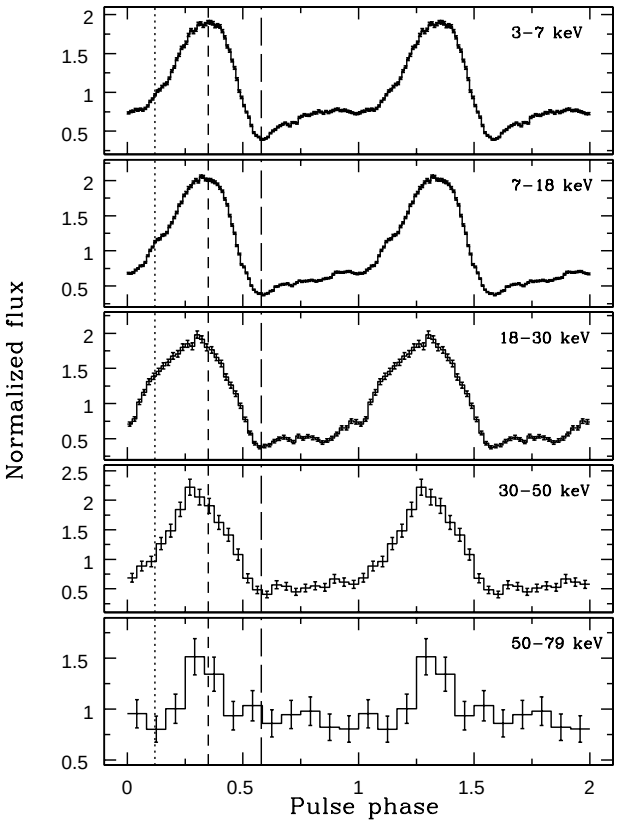

Figure 3. Pulse profiles of 2S 1553−542 as seen by *NuSTAR* in five different energy bands 3–7, 7–18, 18–30, 30–50, and 50–79 keV normalized by the mean flux in each band (from top to bottom). The profiles are plotted twice for clarity. Vertical lines show the positions of the most prominent features: main maximum (short-dashed line), main minimum (long-dashed line) and energy-dependent wing (dotted line).

in 30–50/18–30 keV in contrast to a significant excess in 18–30/7–18 keV and almost ratio of unity in 30–50/7–18 keV bands.

This behaviour is resulted in a wave-like structure of the pulse profile shape as function of energy and is clearly seen in Fig. 5. Dashed line shows the position of the discovered cyclotron line (see Section 3.3). To construct this figure we used pulse profiles normalized by the mean flux value in each energy band, which were chosen to be the same as in Fig. 6.

The pulsed fraction has virtually constant value around 60–70 per cent between 3 and 20 keV, whereas at higher energies it shows a non-monotonic dependence on energy (see Fig. 6). The observed behaviour of the pulsed fraction can be interpreted as local minimum around ∼ 25 keV superimposed on the gradual increase with energy, typical for the majority of X-ray pulsars (Lutovinov & Tsygankov 2009). Note, that only half of all energy bands here are statistically independent, however such representation (equal to a running average) reveals features in the most evident way. At energies above ∼ 40 keV one can observe another decrease of the pulsed fraction. Its possible physical explanation is an influence of the second harmonics of the cyclotron line, which is expected at these energies. However, as can be seen from Fig. 7 the signal from 2S 1553−542 becomes background dominated above 40–50 keV and precise determina-

[2] http://gammaray.msfc.nasa.gov/gbm/science/pulsars.html

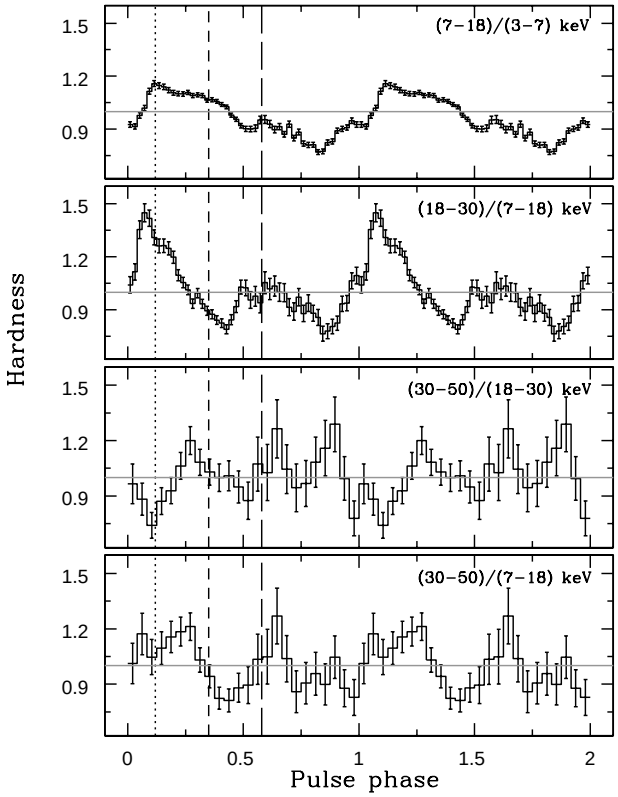

Figure 4. Hardness ratios of 2S 1553−542 pulse profiles in different energy bands (specified in each panel). Vertical lines show the positions of main features in the pulse profile (see Fig. 3). Grey horizontal line represents the hardness ratio of unity.

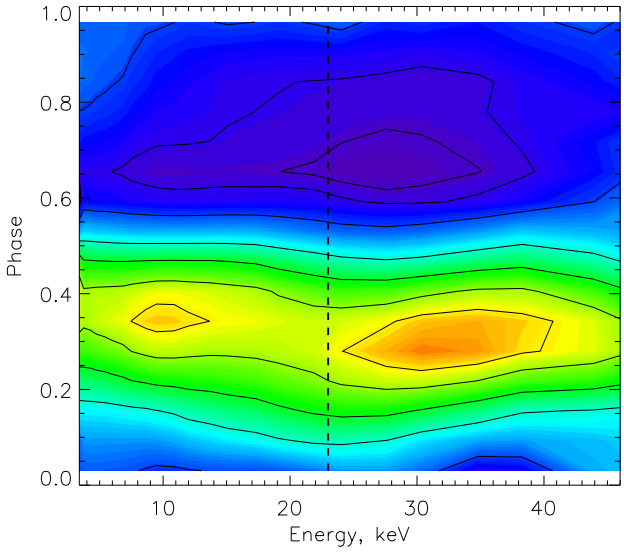

Figure 5. Normalized flux map in the "energy – pulse phase" coordinates. Dashed vertical line shows the position of the cyclotron line centroid energy. Solid contours represent levels of equal normalized flux at 0.45, 0.5, 0.7, 1.1, 1.4, 1.7, 1.9.

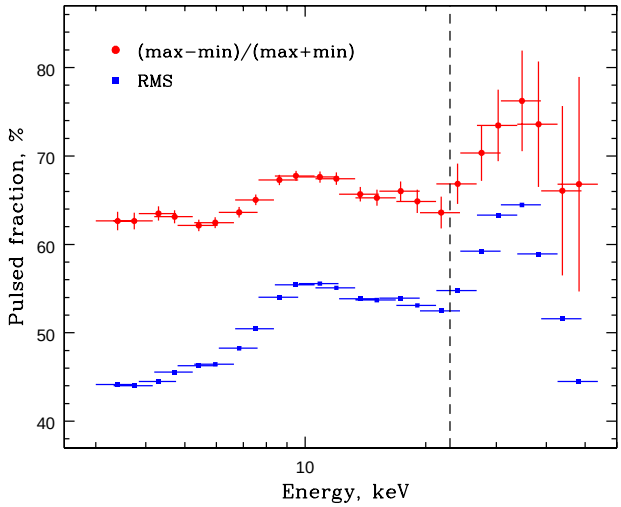

Figure 6. Dependence of the pulsed fraction of 2S 1553−542 on energy obtained using two different approaches (see text for the details) based on the *NuSTAR* data. Dashed line shows the position of CRSF discovered in the source spectrum.

tion of the pulsed fraction depends strongly on the background model. Therefore, the second decrease in the pulsed fraction should be interpreted with caution.

We used two different definitions of the pulsed fraction to avoid any possibly biases due to pulse profile shape or statistics. Standard definition of the pulsed fraction is $\mathrm{PF} = (F_{\max} - F_{\min})/(F_{\max} + F_{\min})$, where $F_{\max}$ and $F_{\min}$ are maximum and minimum fluxes in the pulse profile, respectively. Defined this way pulsed fraction is shown by red circles in Fig. 6. Another approach to characterize flux variations over the pulse is to use the relative Root Mean Square (RMS), which can be calculated using the following equation:

$$RMS = \frac{\left(\frac{1}{N}\sum_{i=1}^{N}(P_i - \langle P\rangle)^2\right)^{\frac{1}{2}}}{\langle P\rangle}, \qquad (3)$$

where P_i is the background-corrected count rate in a given bin of the pulse profile, $\langle P\rangle$ is the count rate averaged over the pulse period, and N is the total number of phase bins in the profile. This definition gives significantly lower absolute value of the pulsed fraction, however all features described above have the same form and are located at the same energies.

3.3 Spectral analysis

The main purpose of the performed *NuSTAR* observations was searching for the cyclotron resonant scattering feature (CRSF) in the source spectrum, measuring its parameters in the case of the discovery or putting strict limits on its presence. The *NuSTAR* observatory is perfectly suitable for these purposes, as it covers uniformly the energy range from 3 to 79 keV (without a necessity to combine different instruments with different response matrixes, like it was for the *RXTE* or *INTEGRAL* observatories) and has an unprecedented sensitivity in the energy range 10–50 keV, where

most of known cyclotron absorption lines were detected (see, e.g., Walter et al. 2015, for a recent review of high mass X-ray binaries). Moreover, good timing capabilities of *NuSTAR* allow to perform the same analysis also for pulse phase resolved spectra, as sometimes cyclotron features are detected only for limited pulse phase intervals and not seen in the pulse averaged spectra. In the following spectral analysis of the source emission we used fixed hydrogen column density 2.3×10^{22} cm^{-2} (Lutovinov et al. 2015b).

3.3.1 *Pulse-phase averaged spectroscopy*

In general, the spectrum of 2S 1553−542 has a shape which is typical for accreting X-ray pulsars and demonstrate an exponential cutoff at high energies (Fig. 7a). Therefore we initially approximated it with the cutoff power-law model (PHABS × CUTOFFPL in the XSPEC package). Results of this fitting give an unacceptable value of $\chi^2 = 3432.1$ for 1303 d.o.f., corresponding residuals are shown in Fig. 7(b). The source and background spectra from both FPMA and FPMB were used for simultaneous fitting, without coadding. To take into account the uncertainty in their calibrations a cross-calibration constant between the modules was added to any used spectral model. From this figure it is clearly seen two peculiarities in the spectrum – an excess at low energies and depression between 20 and 30 keV. An inclusion to the model of an additional black body component (BBODYRAD model in the XSPEC package) with the temperature of about 1 keV improves significantly the fit, but the value of $\chi^2 = 1726.7$ for 1300 d.o.f. is still quite large and associated with the deficit of photons between 20 and 30 keV. Therefore at next step we introduced to the model an absorption component in the form of the CYCLABS model in the XSPEC package. It led to the following improvement of the χ^2 value to 1306.5 for 1297 d.o.f. The corresponding residuals are shown in Fig. 7(c), the line centroid energy is $\simeq 23.5$ keV.

It is worth noticing that the appearance of this feature is not a consequence of the combination of some particular continuum models. We investigated several other spectral models or their combinations to describe the continuum (POWERLAW × HIGHECUT, BBODYRAD + BKNPOWER, COMPTT, BBODYRAD + COMPTT, COMPTT + COMPTT) and found that: 1) all of them approximate it insufficiently well; 2) residuals for all of them demonstrate a prominent absorption-like feature in the 20–30 keV energy range. Thus we can conclude that this absorption feature is real. We interpret this feature as a cyclotron absorption line. Usually two different models, CYCLABS and GABS in the XSPEC package, are used to describe such a feature. Both models adequately approximate an absorption line, but the cyclotron line energy derived from the CYCLABS model is systematically lower (by ∼1–3 keV) than the energy derived from the GABS model (see, e.g., Mihara 1995; Tsygankov et al. 2012; Lutovinov et al. 2015a).

Additionally, the prominent emission feature near 6.4 keV is clearly detected in the source spectrum. This feature is associated with the fluorescent iron emission line and often observed in spectra of BeXRPs. To take it into account we added to the model a corresponding component in the Gaussian form.

Thus the final spectral models which were used for the approximation of the 2S 1553−542 spectrum in the XSPEC package are: PHABS × (BBODYRAD + CUTOFFPL + GAUSS) × CYCLABS (Model I) and PHABS × (BBODYRAD + CUTOFFPL + GAUSS) × GABS (Model II). Their best fit parameters are summarized in Table 2. Note that the normalization of the black body component is proportional to the surface area and depends on the radius of the emission region $R_{\rm bb}$ and distance to the source d as $A = (R_{\rm bb}/d_{10})^2$, where $R_{\rm bb}$ is expressed in km and d_{10} – in units of 10 kpc.

Table 2. Best-fit parameters of the 2S 1553−542 spectrum.

Parameter	Model I	Model II
const	1.015 ± 0.002	1.015 ± 0.002
$N_{\rm H}$, 10^{22} cm^{-2}	2.3	2.3
$kT_{\rm BB}$, keV	0.94 ± 0.02	0.94 ± 0.02
$A_{\rm BB}$[a]	18.7 ± 1.3	19.54 ± 1.3
Photon index	-0.53 ± 0.06	-0.66 ± 0.08
$E_{\rm cut}$, keV	5.59 ± 0.17	5.06 ± 0.10
$\tau_{\rm cycl}$	0.60 ± 0.05	8.28 ± 1.26
$E_{\rm cycl}$, keV	23.46 ± 0.35	27.34 ± 0.38
$\sigma_{\rm cycl}$, keV	10.8 ± 1.0	6.44 ± 0.45
$E_{\rm Fe}$, keV	6.45 ± 0.04	6.45 ± 0.04
$\sigma_{\rm Fe}$, keV	0.41 ± 0.06	0.42 ± 0.06
EW, eV	87 ± 9	89 ± 10
Flux (3–79 keV)[b]	1.025 ± 0.016	1.025 ± 0.016
Flux (3–20 keV)[b]	0.880 ± 0.017	0.880 ± 0.017
χ^2 (d.o.f.)	1306.5(1297)	1301.5(1297)

[a] normalization of the black body component (see text)
[b] in units of 10^{-9} erg s^{-1} cm^{-2}

We are not able to detect the second harmonics of the cyclotron line with the existing data due to the instrumental response drop-off at high energies and high level of the background (see Fig. 7a). The 3σ upper limit on the optical depth of the second harmonics is 1.4 assuming its width being 10 keV. More observational data or other instruments are needed to make a final conclusion about its presence in the spectrum.

3.3.2 *Pulse-phase resolved spectroscopy*

As it was mentioned above, spectra of X-ray pulsars can vary significantly over the pulse. The observed variations of spectral parameters can give information about changes of the physical conditions or parameters of the emission regions near the neutron star. In order to study their evolution over the pulse period in the case of 2S 1553−542 we performed a pulse-phase resolved spectroscopy. The spin period was divided into 10 equal phase bins. The pulse profile has a more or less smooth shape (Fig. 3), therefore such a division allows us both to obtain a good statistic for each spectrum and to trace well evolution of spectral parameters.

To describe phase-resolved spectra we used the same spectral model as for the analysis of the averaged spectrum (with CYCLABS prescription for the cyclotron line; Model I). It is necessary to note that the width of the cyclotron line cannot be firmly determined in some phase bins due to insufficient photon statistics. Therefore, its value was fixed at 8 keV – the value which was measured in phase bins near the pulse maximum with the better statistics.

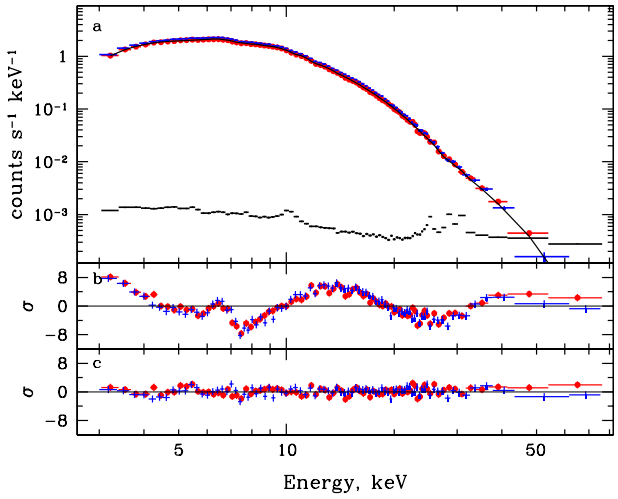

Figure 7. (a) Pulse phase averaged spectrum of 2S 1553−542 obtained with the *NuSTAR* observatory. Red circles and blue crosses correspond to FPMA and FPMB modules data, respectively. The black line shows the best fit by the model consist of PHABS × (BBODYRAD + CUTOFFPL + GAUSS) × CYCLABS. (b) Residuals from the PHABS × CUTOFFPL continuum model. (c) Residuals from PHABS × (BBODYRAD + CUTOFFPL + GAUSS) × CYCLABS model. Black crosses represent averaged background level.

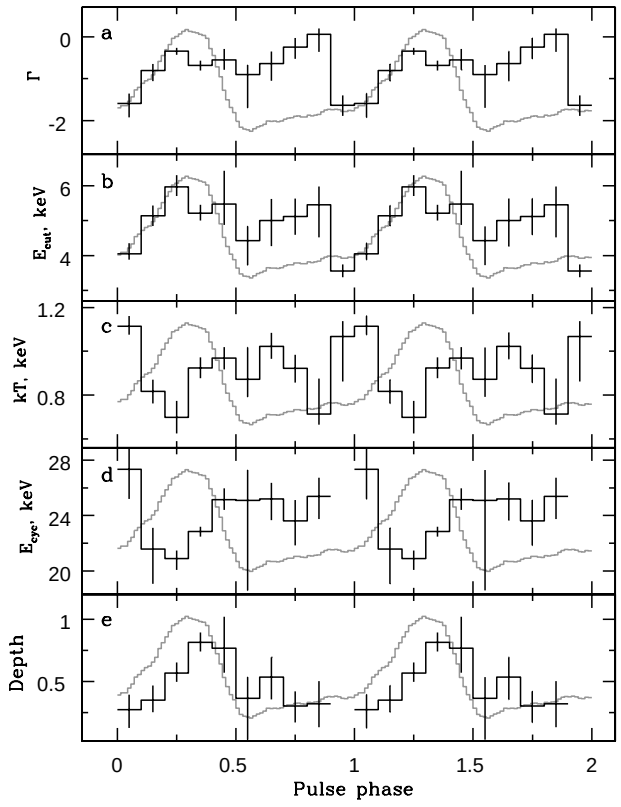

Figure 8. Spectral parameters of the best-fit model (Model I, see text) as a function of pulse phase. The black histogram in the panels represents: (a) photon index, (b) cutoff energy, (c) black body temperature, (d) cyclotron line energy, (e) cyclotron line depth. Grey line in each panel shows pulse profile in wide energy range. The cyclotron line is not detected in the 10th bin.

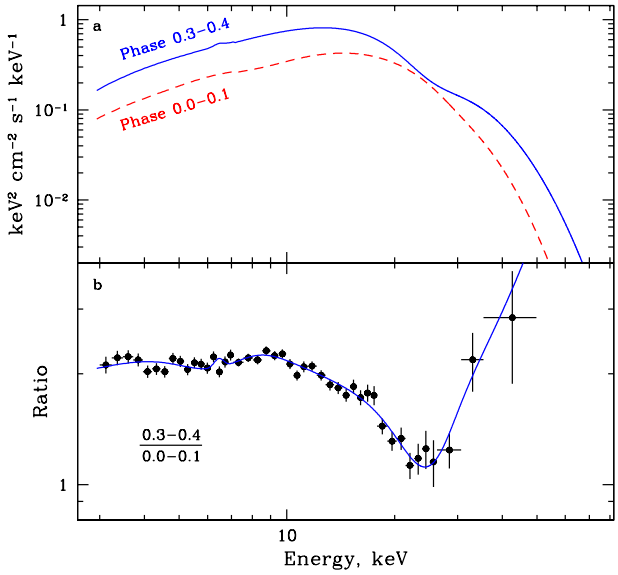

Figure 9. (a) Best fit spectral models for two different phase bins. Red dashed line and blue solid line represent phases 0.0–0.1 and 0.3–0.4, correspondingly. Their ratio is shown in panel (b). Prominent absorption-like feature is seen between 20 and 30 keV.

The results of the pulse phase-resolved spectroscopy are shown in Fig. 8. The average pulse profile of 2S 1553−542 across the entire *NuSTAR* energy range is presented in each panel to visualize better the variations of spectral parameters with the phase. The photon index is varying quite significantly (from –2 to 0) whereas the cutoff energy is less variable staying in the range between 4 and 6 keV. We can mention also a possible tentative correlation between these parameters. The temperature of the black body component is around $\simeq$ 1 keV and is quite stable over the pulse with some variations from $\sim$ 1.1 to $\sim$ 0.7 keV in first three bins.

Variations of the cyclotron line energy and the line depth are the most interesting and important for us, as both of them are changing significantly over the pulse. In particular, the line centroid energy has minimum ($E_{\rm cycl} \simeq 21$ keV) near the pulse profile maximum, whereas the line depth has maximum near this phase. In general, the line energy $E_{\rm cycl}$ is varying between $\simeq$ 21 and $\simeq$ 27 keV (using CYCLABS model for the cyclotron line), that is the main reason for the significant broadening of the line measured in the averaged spectrum ($\sim$ 11 keV). Note that the described behaviour of the cyclotron line parameters over the pulse is very similar to the observed one in well studied BeXRP V 0332+53 when this object had nearly the same luminosity $L \simeq 6 \times 10^{37}$ erg s^{-1} (Lutovinov et al. 2015a). From another side this behaviour is opposite to what observed in sub-critical pulsars due to different beaming properties (see, e.g., Klochkov et al. 2008, for the X-ray pulsar Her X-1).

To demonstrate that the observed spectral variations are real ones we show the ratio of two spectra obtained in the first (minimal line depth) and forth (maximal line depth) phase bins in Fig. 9. The upper panel demonstrates corresponding models for these spectra. The ratio of the observed spectra is shown in the bottom panel with filled circles. The solid line in this panel represents the ratio of the corresponding models. A strong absorption like feature, caused by dif-

ference in line depths for these phase bins is clearly seen in this figure between 20 and 30 keV.

The contribution of different continuum components (black body and power-law with cutoff) to the total source luminosity demonstrates a variability of their ratio over the pulse. Particularly, the black body flux remains virtually constant at the level of $\sim 9 \times 10^{-11}$ erg s^{-1} cm^{-2}, whereas power-law flux is dominating at all phases and is determining the overall pulse profile shape. The contribution of the black body emission to the total flux is varying between ~ 5 and ~ 15 per cent. Using estimation of the distance to the source $d \sim 20$ kpc (see Section 4) the measured black body flux corresponds to the emitting area with the radius of $R \sim 9$ km. This value is comparable with the neutron star size, that means that the black body emission can emerge from the neutron star atmosphere heated up by the intercepted emission from the accretion column (Poutanen et al. 2013). So big radius of the illuminated NS surface area can explain virtual constancy of the black body emission component over the pulse. This hypothesis can be verified in future by a set of observations of 2S 1553−542 at different luminosities and, hence, with different illuminated areas on the neutron star.

4 DISCUSSION

In this work we presented detailed spectral and temporal analysis of the emission from the poorly studied BeXRP 2S 1553−542 using the *NuSTAR* data collected during the presumably Type II outburst in 2015. The energy spectrum of the source cannot be fitted satisfactory with any simple continuum model but requires inclusion of the absorption feature centered at ~ 23.5 keV.

This absorption component has a clear physical meaning and represents the cyclotron absorption line known to be main evidence for the strong magnetic field on the neutron star surface (Gnedin & Sunyaev 1974). The absorption line in the 2S 1553−542 spectrum can be fitted both by the Gaussian (GABS model) or Lorenzian (CYCLABS model) profiles with approximately the same quality. The line energy ($\simeq 27.3$ keV for GABS and $\simeq 23.5$ keV for CYCLABS) corresponds to the magnetic field strength at the neutron star surface $B \sim 3 \times 10^{12}$ G after the correction for the gravitational redshift.

The existence of the cyclotron feature is confirmed not only by the spectral fitting, but also by temporal properties of the source. Particularly, the pulsed fraction dependence on the energy has a broad feature (local decrease) around 23 keV (see Fig. 6) that coincides with the position of CRSF in the source spectrum. Such non-monotonic dependencies of the pulsed fraction on energy were observed in several X-ray pulsars with cyclotron line in their spectra (Lutovinov & Tsygankov 2009; Ferrigno et al. 2009) and even were proposed as a tool to search for CRSFs.

Further evidence for the cyclotron absorption feature comes from the behaviour of the pulse profile with energy. A phase lag around the spectral feature can be clearly seen in Figs 3 and 5 expressed in a wave-like structure near 20–30 keV. Such behaviour has been shown to be typical for a few others transient BeXRPs (Tsygankov et al. 2006, 2007; Iyer et al. 2015) and can be explained by a natural assumption of an energy-dependent beaming of the radiation from the emitting region (Ferrigno et al. 2011; Schönherr et al. 2014).

The knowledge of the magnetic field strength gives us an opportunity to estimate the absolute value of the mass accretion rate needed to provide the spin-up rate measured by *Fermi*/GBM at the moment of our *NuSTAR* observation $\dot{P} = -(7.5 \pm 0.9) \times 10^{-10}$ s s^{-1}. For that we used the accretion torque theories developed by different authors (Ghosh & Lamb 1979; Wang 1995; Kluźniak & Rappaport 2007). These models explain the observed spin-up/down rate as a function of the neutron star parameters and depend on physics of "accretion disc – magnetosphere" interaction. For our calculations we used the NS magnetic dipole moment $\mu = 1.5 \times 10^{30}$ G cm^3, derived from the measured value of the magnetic field strength, $1.4 M_\odot$ and 10 km as the neutron star mass and radius, respectively, keeping the mass accretion rate as a free parameter.

Type II outbursts in BeXRPs are usually accompanied by the formation of the temporary accretion disk around the neutron star (see, e.g., Reig 2011, and references therein) revealing itself in a strong spin-up rate and properties of the noise power spectrum (Revnivtsev et al. 2009). Therefore, as a first approximation we used eq. (15) from Ghosh & Lamb (1979) to estimate the bolometric luminosity $L = (7.6 \pm 0.9) \times 10^{37}$ erg s^{-1} needed to support the measured spin-up rate. Given the flux from 2S 1553−542 during the *NuSTAR* observation $F = 1.05 \times 10^{-9}$ erg s^{-1} cm^{-2} the distance to the system can be estimated as $d \sim 22$ kpc.

The torque model by Ghosh & Lamb (1979) is not the only one developed for the disc accretion. In all these models the total torque can be expressed in the form $N_{\rm tot} = n(\omega_s) N_{\rm acc}$. The only parameter of the dimensionless angular momentum $n(\omega_{\rm s})$ is so called fastness parameter $\omega_{\rm s} = (r_{\rm m}/r_{\rm co})^{3/2}$, where $r_{\rm m}$ and $r_{\rm co}$ are magnetospheric and corotation radii, correspondingly. We used different prescriptions for the dimensionless angular momentum $n(\omega_s)$ which describes physical properties of the accretion disc interaction with the magnetosphere. Particularly, utilizing approaches from Kluźniak & Rappaport (2007) and Wang (1995) we got distances $d \sim 17$ kpc and $d \sim 22$ kpc, correspondingly. Such not large dispersion of the distances derived from different models is due to the source being far from the spin equilibrium, where the difference in the above-mentioned models is maximal (see, e.g., Fig. 2 from Parfrey, Spitkovsky, & Beloborodov 2015).

Radius of the magnetosphere in these models is assumed to be a fraction of the Alfvén radius $r_{\rm m} = \xi r_{\rm A}$. In the calculations above we assumed the parameter $\xi = 0.5$, however its exact value is not known and supposed to be between 0.5 and 0.7 (see, e.g., Parfrey, Spitkovsky, & Beloborodov 2015, and references therein). To estimate a possible influence of this parameter for our results we recalculated distances with $\xi = 0.7$. This affected the derived values very insignificantly shifting the distance estimations based on models by Ghosh & Lamb (1979) and Wang (1995) to ∼24 and ∼21 kpc, respectively. These estimations make 2S 1553−542 one of the most distant high-mass X-ray binary in the Galaxy (Lutovinov et al. 2013), putting it to the opposite side of the Milky Way. It is important to note, that the distance estimations based on the temporal properties of X-ray pulsars have quite large systematic uncertainties (of the order of 15–20

per cent) due to model dependency, an unknown efficiency of the accretion and effects of a possible emission beaming, therefore should be considered with the caution. Nevertheless, a large distance to the source (>15 kpc) is estimated from the optical data as well (Lutovinov et al. 2015b).

The dispersion of the estimated distance values can be considered as a systematic uncertainty of this method. It is interesting to note, that if our estimations of distance (20 ± 4 kpc) are correct then 2S 1553−542 exceeds the so-called critical luminosity above which the accretion column begins to grow above the neutron star surface (Basko & Sunyaev 1976). The value of the critical luminosity as well as conditions for growing of the accretion column are still under debates and depend on the physical models (see, e.g., Mushtukov et al. 2015, and references therein). A set of observations in different intensity states during the outburst is needed to verify this hypothesis by, e.g., observing of the anti-correlation between the cyclotron energy and source luminosity, as seen in at least one bright transient X-ray pulsar V 0332+53 (Mihara, Makishima, & Nagase 1998; Tsygankov et al. 2006; Tsygankov, Lutovinov, & Serber 2010). Presence of such an anti-correlation in another similar source, 4U 0115+63, is still under debates (Nakajima et al. 2006; Tsygankov et al. 2007; Müller et al. 2013; Boldin, Tsygankov, & Lutovinov 2013).

5 CONCLUSION

The recent outburst from BeXRP 2S 1553−542 was only the third transient event when the source came into the view of X-ray instruments. Thanks to the *NuSTAR* wide energy coverage and high sensitivity we were able to discover a cyclotron absorption line with centroid energy $E_{\rm cyc} = 23.5 \pm 0.4$ keV, corresponding to the neutron star magnetic field strength $B \sim 3 \times 10^{12}$ G typical for the known X-ray pulsars (Walter et al. 2015). The presence of the cyclotron line in the source spectrum is also supported by the behaviour of the pulse profile and pulsed fraction with the energy.

The pulse-phase resolved spectroscopy revealed significant variations of the cyclotron line parameters over the pulse. Particularly, the line centroid energy is anti-correlating with the intensity, whereas the line depth shows a correlation.

Thanks to the *Fermi*/GBM data we were able to substantially improve the orbital parameters of the system. The intrinsic spin period value and its evolution observed by *Fermi*/GBM and *NuSTAR* during the current outburst are similar to those measured by the *RXTE* observatory during the previous outburst (Pahari & Pal 2012). Virtual constancy of the period since the source discovery in 1975 and a significant spin-up observed during both outbursts (up to $\dot{P} \sim -10^{-9}$ s s^{-1}) implies action of deceleration torques between outbursts. Taking into account the last measured value of the pulse period during the previous outburst (Pahari & Pal 2012) and its first measured value during the current outburst (Fig. 1) we can estimate roughly a spin-down between 2007 and 2015 outbursts as $\dot{P} \sim (3{-}4)\times10^{-11}$ s s^{-1}. This value is more than an order of magnitude lower than the spin-up during the outbursts and comparable with the spin-down observed between outbursts in other BeXRBs (see, e.g., Postnov et al. 2015).

The knowledge of the magnetic field and spin-up rate allowed us to estimate the distance to the system $d = 20\pm4$ kpc using the standard accretion torque models. So large distance agrees well with the fact that the optical counterpart was not directly detected so far.

ACKNOWLEDGMENTS

This research has made use of data obtained with *NuSTAR*, a project led by Caltech, funded by NASA and managed by NASA/JPL, and has utilized the NUSTARDAS software package, jointly developed by the ASDC (Italy) and Caltech (USA). This research has made also by using *Chandra* data provided by the Chandra X-ray Center. The publication makes use of software provided by the Chandra X-ray Center (CXC) in the application package CIAO. ST, AL and SM acknowledge support from Russian Science Foundation (grant 14-12-01287). JP thanks the Academy of Finland for financial support (grant 268740). Partial support comes from the EU COST Action MP1304 "NewCompStar".

REFERENCES

An H., et al., 2014, SPIE, 9144, 91441Q
Basko M. M., Sunyaev R. A., 1976, MNRAS, 175, 395
Becker P. A., et al., 2012, A&A, 544, A123
Boldin P. A., Tsygankov S. S., Lutovinov A. A., 2013, AstL, 39, 375
Boyd P. T., Still M., Kennea J., Krimm H. A., 2008, ATel, 1371, 1
Deeter J. E., Boynton P. E., Pravdo S. H., 1981, ApJ, 247, 1003
Dickey J., Lockman F., 1990, ARA&A, 28, 215
Ferrigno C., Becker P. A., Segreto A., Mineo T., Santangelo A., 2009, A&A, 498, 825
Ferrigno C., Falanga M., Bozzo E., Becker P. A., Klochkov D., Santangelo A., 2011, A&A, 532, A76
Finger M. H., Bildsten L., Chakrabarty D., Prince T. A., Scott D. M., Wilson C. A., Wilson R. B., Zhang S. N., 1999, ApJ, 517, 449
Ghosh P., Lamb F. K., 1979, ApJ, 234, 296
Gnedin I. N., Sunyaev R. A., 1974, A&A, 36, 379
Harrison F. A., et al., 2013, ApJ, 770, 103
Iyer N., Mukherjee D., Dewangan G. C., Bhattacharya D., Seetha S., 2015, MNRAS, 454, 741
Jenke P. A., Finger M. H., Wilson-Hodge C. A., Camero-Arranz A., 2012, ApJ, 759, 124
Kalberla P., Burton W., Hartmann D., Arnal E., Bajaja E., Morras R., Pppel W., 2005, A&A, 440, 775
Kelley R. L., Ayasli S., Rappaport S., 1982, IAUC, 3667, 3
Kelley R. L., Rappaport S., Ayasli S., 1983, ApJ, 274, 765
Klochkov D., et al., 2008, A&A, 482, 907
Kluźniak W., Rappaport S., 2007, ApJ, 671, 1990
Krimm H. A., et al., 2007, ATel, 1345, 1
Krimm H. A., et al., 2013, ApJS, 209, 14
Krivonos R. A., et al., 2015, ApJ, 809, 140
Lutovinov A. A., Tsygankov S. S., 2009, AstL, 35, 433
Lutovinov A. A., Revnivtsev M. G., Tsygankov S. S., Krivonos R. A., 2013, MNRAS, 431, 327
Lutovinov A. A., Tsygankov S. S., Suleimanov V. F., Mushtukov A. A., Doroshenko V., Nagirner D. I., Poutanen J., 2015a, MNRAS, 448, 2175

Lutovinov A. et al., 2015b, MNRAS, submitted
Meegan C., et al., 2009, ApJ, 702, 791
Mihara T., 1995, PhD thesis, Dept. of Physics, Univ. of Tokyo
Mihara T., Makishima K., Nagase F., 1998, AdSpR, 22, 987
Müller S., et al., 2013, A&A, 551, A6
Mushtukov A. A., Suleimanov V. F., Tsygankov S. S., Poutanen J., 2015, MNRAS, 447, 1847
Nakajima M., Mihara T., Makishima K., Niko H., 2006, ApJ, 646, 1125
Pahari M., Pal S., 2012, MNRAS, 423, 3352
Parfrey K., Spitkovsky A., Beloborodov A. M., 2015, arXiv, arXiv:1507.08627
Postnov K. A., Mironov A. I., Lutovinov A. A., Shakura N. I., Kochetkova E. A., Tsygankov S. S., 2015, MNRAS, 446, 1013
Poutanen J., Mushtukov A. A., Suleimanov V. F., Tsygankov S. S., Nagirner D. I., Doroshenko V., Lutovinov A. A., 2013, ApJ, 777, 115
Reig P., 2011, Ap&SS, 332, 1
Rappaport S., Joss P. C., 1977, Natur, 266, 123
Revnivtsev M., Churazov E., Postnov K., Tsygankov S., 2009, A&A, 507, 1211
Schönherr G., et al., 2014, A&A, 564, L8
Standish E. M., Jr., 1990, A&A, 233, 252
Sugizaki M., et al., 2015, ATel, 7018, 1
Tsygankov S. S., Lutovinov A. A., Churazov E. M., Sunyaev R. A., 2006, MNRAS, 371, 19
Tsygankov S. S., Lutovinov A. A., Churazov E. M., Sunyaev R. A., 2007, AstL, 33, 368
Tsygankov S. S., Lutovinov A. A., Serber A. V., 2010, MNRAS, 401, 1628
Tsygankov S. S., Krivonos R. A., Lutovinov A. A., 2012, MNRAS, 421, 2407
Walter F., 1976, IAUC, 2959, 2
Walter R., Lutovinov A. A., Bozzo E., Tsygankov S. S., 2015, Astronomy and Astrophysics Review, 23, 2 [arXiv:1505.03651]
Wang Y.-M., 1995, ApJ, 449, L153
Wik D. R., et al., 2014, ApJ, 792, 48

This paper has been typeset from a TEX/LATEX file prepared by the author.